A [89]Zr-HDL PET tracer monitors response to a CSF1R inhibitor

[89]Zr-HDL tracer guides CSF1R therapy

Christian A. Mason[1], Susanne Kossatz[1], Lukas M. Carter[1], Giacomo Pirovano[1], Christian Brand[1], Navjot Guru[1], Carlos Pérez-Medina[4,8], Jason S. Lewis[1,2,3], Willem J.M. Mulder[4,5,6,7] and Thomas Reiner[1,3,9,10*]

Affiliations:

[1]Department of Radiology, Memorial Sloan Kettering Cancer Center, New York, NY, 10065, USA.
[2]Molecular Pharmacology Program, Memorial Sloan Kettering Cancer Center, New York, NY, 10065, USA.
[3]Department of Radiology, Weill Cornell Medical College, New York, NY, 10065, USA
[4]Translational and Molecular Imaging Institute, Icahn School of Medicine at Mount Sinai, New York, NY, 10029, USA
[5]Department of Oncological Sciences, Icahn School of Medicine at Mount Sinai, New York, NY, 10029
[6]Laboratory of Chemical Biology, Department of Biomedical Engineering and Institute for Complex Molecular Systems, Eindhoven University of Technology, Eindhoven, Netherlands
[7]Department of Medical Biochemistry, Amsterdam University Medical Centers, Academic Medical Center, Amsterdam, Netherlands.
[8]Centro Nacional de Investigaciones Cardiovasculares Carlos III, Madrid, Spain
[9]Chemical Biology Program, Memorial Sloan Kettering Cancer Center, New York, NY, 10065, USA
[10]Center for Molecular Imaging and Nanotechnology (CMIT), Memorial Sloan Kettering Cancer Center, New York, NY, 10065, USA

Corresponding author:
Thomas Reiner
Memorial Sloan Kettering Cancer Center
1275 York Avenue, New York, 10065, NY, USA
Phone: 646 888 3461; Email: Reinert@mskcc.org; Fax:646 422 0408

ABSTRACT

The immune function within the tumor microenvironment has become a prominent therapeutic target, with tumor-associated macrophages (TAMs) playing a critical role in immune suppression. We propose an ^{89}Zr-labeled high-density lipoprotein (^{89}Zr-HDL) nanotracer as a means of monitoring response to immunotherapy.

Methods: Female MMTV-PyMT mice were treated with pexidartinib, a colony-stimulating factor 1 receptor (CSF1R) inhibitor, to reduce TAM density. The accumulation of ^{89}Zr-HDL within the tumor was assessed using PET/CT imaging and autoradiography, whereas TAM burden was determined using immunofluorescence.

Results: A significant reduction in ^{89}Zr-HDL accumulation was observed in PET/CT images, with 2.9 ± 0.3 %ID/g and 3.7 ± 0.2 %ID/g for the pexidartinib- and vehicle-treated mice, respectively. This reduction was corroborated *ex vivo* and correlated with decreased TAM density.

Conclusion: These results support the potential use of ^{89}Zr-HDL nanoparticles as a PET tracer that could quickly monitor the response to CSF1R inhibitors and other therapeutic strategies targeting TAMs.

Keywords: Immunotherapy, tumor-associated macrophages, PET/CT imaging, CSF1R inhibitor, HDL

INTRODUCTION

Breast cancer is the second leading cause of cancer-related death for women in the United States. Mortality in breast cancer results from the formation of metastases in organs such as the brain, liver, lungs, and bone marrow (*1*). Although a large majority of patients do not present with metastatic lesions in distant tissue upon initial diagnosis, one in three women with node-negative and an even larger percentage of those with node-positive breast cancer will eventually develop distant metastases (*2*). The standard of care for early and late stage breast cancers includes chemotherapy, radiation therapy, or endocrine therapy (*3*). While the 5-year survival rate for breast cancer is near 90%, the rate significantly decreases to 30% in metastatic breast cancer (*4*). An appreciable amount of research has described the critical roles that the innate and adaptive immune system plays in cancer development and progression (*5,6*). Immune checkpoint blockade, engineered chimeric antigen receptor (CAR) T cells, and other drugs designed to modulate the activity and migration of innate and adaptive immune cells have become focal points of preclinical and clinical research (*7*).

The recruitment of myeloid cells, in particular macrophages, is considered to be one of the earliest and most crucial phases in the development of metastatic lesions (*2*). Macrophages exhibit dual functionality in modulating immune response, "classically activated" are pro-inflammatory, while "alternatively activated" macrophages secrete cytokines that induce tissue repair and suppress immune function (*8*). The accumulation of macrophages within the tumor and their shift towards an alternatively activated phenotype results in signaling cascades that induce angiogenesis, alter the extracellular matrix, and suppress adaptive immune response (*9–11*). Therefore, TAM burden has been correlated with rapid tumor growth, metastatic potential, and poor patient prognosis (*12*).

Colony-stimulating factor 1 (CSF1) and its respective receptor (CSF1R), play a key role in the recruitment and activation of macrophages (*13*). There are numerous clinical trials exploring the use of CSF1R inhibitors as a monotherapy or in combination with other therapeutic strategies in various types of cancer (*14*). Pexidartinib (PLX3397), a CSF1R inhibitor currently in phase 3 clinical trials, has shown promising results as a monotherapy and in combination with immune checkpoint therapies (*14*). However, traditional methods of evaluating patient response can provide misleading results. Thus, physicians require approximately 3-4 months to properly assess the treatments efficacy in patients undergoing immunotherapies (*15*).

The affinity of high-density lipoprotein (HDL) particles for macrophages has been well documented, and numerous formulations have been engineered to non-invasively visualize macrophage accumulation in a variety of inflammatory diseases such as atherosclerosis, arthritis, and cancers using different imaging modalities (*16–20*). Here, we explore the use of [89]Zr-labeled reconstituted HDL as a macrophage-targeted diagnostic tool that could help clinicians to more quickly and accurately assess the response to anti-TAM immunotherapies. In order to evaluate the [89]Zr-HDL's ability to non-invasively monitor TAM-burden by positron emission tomography (PET), we chose an aggressive transgenic mouse model of mammary adenocarcinoma: MMTV-PyMT (*21*). [89]Zr-HDL nanoparticles' biodistribution, specifically accumulation in the tumor, was analyzed and compared in pexidartinib-treated and untreated MMTV-PyMT mice (Supplementary Figure 1).

RESULTS

Synthesis and Radiolabeling of HDL Nanoparticles

^{89}Zr-labeled HDL nanoparticles were prepared following our previously reported methods (*18*) (Figure 1A). DFO-HDL nanoparticles had a hydrodynamic diameter of 10.9 ± 2.8 nm (n=3), as determined by DLS (Figure 1B). ^{89}Zr-HDL nanoparticles were isolated in a 93% ± 6% (n=3) radiochemical yield and greater than 99% radiochemical purity, as determined by radio-HPLC (Figure 1C).

PET/CT Imaging and In Vivo Quantification of ^{89}Zr-HDL Nanoparticles

In order to assess the ability of the ^{89}Zr-HDL nanoparticles to act as a macrophage tracer to monitor CSF1R inhibition, MMTV-PyMT mice were treated with PLX3397 or vehicle for 5 days via daily oral gavage. This particular strain of mice begin to spontaneously develop mammary adenocarcinomas as early as 3 weeks old (*21*). At approximately 11 weeks of age, when the mammary tumors had grown to an average size of 0.5 cm in diameter, the treatment was initiated. Administration of PLX3397 and vehicle was performed for 5 days based on previously reported results (*13*). The mice were then administered the ^{89}Zr-HDL nanoparticles and imaged 24 hours post injection. ^{89}Zr-HDL uptake in tumors, determined non-invasively by drawing volumes of interest over the entire tumor mass within the mammary glands on the PET/CT images (Supplemental Figure 2), was significantly lower in PLX3397-treated mice compared to controls (2.9 ± 0.3 %ID/g vs. 3.7 ± 0.2 %ID/g, P < 0.01, Figure 3B).

Ex Vivo Quantification of ^{89}Zr-HDL Nanoparticles and Macrophage burden

Mice were sacrificed immediately following PET/CT imaging and the tumors were harvested, frozen in OCT, and sectioned for immunofluorescence and autoradiographic analysis. Quantification of macrophage burden was performed through IBA-1 staining

followed by immunofluorescence imaging, with observed macrophage densities of 3.1 ± 0.9 % IBA-1 positive cells and 12.3 ± 6.4 % IBA-1 positive cells for PLX3397 and vehicle treated mice, respectively (P < 0.05, Figure 2B). In addition, the ^{89}Zr-HDL nanoparticle accumulation was assessed using autoradiography and normalized to the injected dose. This analyses showed a significantly lower radioactivity deposition in tumors from PLX3397-treated mice compared to controls (11.3 ± 1.2 Max A.U./ID vs. 15.8 ± 3.2 Max A.U./ID, P < 0.05, Figure 2C). The differences in nanoparticle accumulation, as observed in both *in vivo* and *ex vivo* analyses, correlates with the changes in TAM density as a result of CSF1R inhibition (*22,23*).

DISCUSSION

The purpose of this study was to evaluate the use of an [89]Zr-HDL nanoparticle as a macrophage tracer that could provide clinicians an additional tool to assess the effect of CSF1R inhibitors and other immunotherapies on TAMs. The intricate role TAMs play in altering immune function within the tumor microenvironment has made them of particular interest as targets in numerous therapeutic studies (*11,14*). The combination of therapeutic strategies altering both the innate and adaptive immune system is promising, however there are currently no accepted biomarkers that can accurately predict immunotherapy efficacy (*7*). Traditional methods such as Response Evaluation Criteria in Solid Tumors (RECIST) can be misleading when evaluating patients undergoing immunotherapy as tumor size can vary with changes in immune cell infiltration (*15,24,25*). This phenomena, known as pseudoprogression, prevents physicians from contemporaneously assessing therapeutic responses, delaying conclusive evaluation to at least 3-4 months after treatment initiation (*26,27*). Therefore, a significant clinical need exists to develop methods that can quickly and accurately monitor the effect these therapies have on TAM populations.

The observed [89]Zr-HDL uptake assessed through *in vivo* PET/CT and *ex vivo* autoradiography analyses showed significant differences between PLX3397- and vehicle-treated cohorts. The excised tumors included areas of high fat content, as they were collected from the mammary fat pad, making it difficult to draw ROI's that included only the cancer cells and stroma. When the activity was averaged over the drawn ROI, a decrease in nanoparticle accumulation as a result of PLX3397 treatment was observed (Supplemental Figure 3B). However, the differences in accumulation between the two groups was not statistically significant. Thus, the maximum accumulated activity within each tissue section was also analyzed in order to reduce the impact areas with high fat content and very low nanoparticle accumulation had on the analysis. The resulting data

7

for the excised tumors showed statistically significant differences in ^{89}Zr-HDL nanoparticles between the two cohorts (Figure 2C). The immunofluorescence analysis provided evidence of effective reduction in macrophage density within the tumor as a result of the CSF1R inhibition. In addition, while IBA-1 is a prominently used macrophage stain in immunofluorescence, it's expression is not exclusive to macrophages (28). IBA-1 can also appear on other myeloid cells such as monocytes and some lymphocytes. CSF1R inhibition, using PLX3397, was shown to be ineffective at reducing infiltration of monocytes and dendritic cells in the PYMT-MMTV mouse model (13). Thus any IBA-1 staining associated with these cell populations may have led to smaller observed differences in TAM populations between the PLX3397- and vehicle- treated cohorts (13). While there was considerable variation in TAM density between tissue sections, illustrating the highly heterogenous nature of the tumor microenvironment, the differences between the PLX3397- and vehicle- treated cohorts remained statistically significant (Figure 2B). A correlation between macrophage density and ^{89}Zr-HDL nanoparticle accumulation was observed in both the PET/CT and *ex vivo* analyses (Supplementary Figure 3). As is apparent in the PET/CT images there was significant accumulation of the ^{89}Zr-HDL nanoparticles within the liver (Figure 3A). Thus, while the tracer is ostensibly capable of imaging tumors in most tissues, the ^{89}Zr-HDL nanoparticles would likely be unable to delineate metastases within the liver. The observed differences in nanoparticle accumulation, assessed using both *in vivo* PET/CT imaging and *ex vivo* autoradiography, were the result of modulations in TAM density as a consequence of treatment with the CSF1R inhibitor, pexidartinib. As observed in the *ex vivo* analysis the macrophage content and nanoparticle accumulation was very heterogeneous. The use of PET/CT was able to overcome this heterogeneity, as ^{89}Zr-HDL nanoparticle accumulation provided a quantifiable means of evaluating TAM content over the entire tumor area. Thus, the use of ^{89}Zr-HDL nanoparticles as a macrophage avid PET-tracer provides a non-invasive tool

8

to quantitatively assess overall macrophage burden and could provide clinicians the means to quickly and accurately assess response to macrophage targeted therapies.

CONCLUSION

The data presented herein shows that ^{89}Zr-HDL tumor uptake correlates with macrophage density within the tumor microenvironment. The statistically significant modulation in TAM burden, as a result of PLX3397 treatment, could be observed by quantifiable differences in ^{89}Zr-HDL nanoparticle uptake using PET imaging within one week of initiating treatment. Thus, ^{89}Zr-HDL nanoparticles are a promising tool that could potentially help physicians more rapidly and accurately determine the early response to therapies targeting the immunosuppressed tumor microenvironment.

ACKNOWLEDGEMENTS

DISCLOSURE

There are no conflicts of interest.

SUPPORTING INFORMATION DESCRIPTION

Supplementary File 1 contains additional methods description.

Supplementary Fig. contains Supplementary Figure 1, 2, and 3.

REFERENCES

1. Guo F, Kuo Y, Shih YCT, Giordano SH, Berenson AB. Trends in breast cancer mortality by stage at diagnosis among young women in the United States. *Cancer*. 2018;124:3500-3509.

2. Kimbung S, Loman N, Hedenfalk I. Clinical and molecular complexity of breast cancer metastases. *Semin Cancer Biol*. 2015;35:85-95.

3. Treatment of Stage IV (Metastatic) Breast Cancer. https://www.cancer.org/cancer/breast-cancer/treatment/treatment-of-breast-cancer-by-stage/treatment-of-stage-iv-advanced-breast-cancer.html.

4. Cancer of the Breast (Female) - Cancer Stat Facts. https://seer.cancer.gov/statfacts/html/breast.html.

5. Eichten A, Visser KE de, Coussens LM. Paradoxical roles of the immune system during cancer development. *Nat Rev Cancer*. 2006;6:24.

6. Marx J. Inflammation and cancer: the link grows stronger: research into a long-suspected association between chronic inflammation and cancer reveals how the immune system may be abetting tumors. *Science*. 2004;306:966-969.

7. Havel JJ, Chowell D, Chan TA. The evolving landscape of biomarkers for checkpoint inhibitor immunotherapy. *Nat Rev Cancer*. 2019;19:133.

8. Murray PJ. Macrophage Polarization. *Annu Rev Physiol*. 2017;79:541-566.

9. Marelli G, Allavena P, Erreni M. Tumor-associated macrophages, multi-tasking cells in the cancer landscape. *Cancer Res Front*. 2015;1:149-161.

10. Chanmee T, Ontong P, Konno K, Itano N. Tumor-associated macrophages as major players in the tumor microenvironment. *Cancers*. 2014;6:1670-1690.

11. Soloff AC, Williams CB, Yeh ES. Tumor-associated macrophages: unwitting accomplices in breast cancer malignancy. *Npj Breast Cancer*. 2016;2:15025.

12. Zhao X, Qu J, Sun Y, et al. Prognostic significance of tumor-associated macrophages in breast cancer: a meta-analysis of the literature. *Oncotarget*. 2017;8:30576-30586.

13. DeNardo DG, Brennan DJ, Rexhepaj E, et al. Leukocyte Complexity Predicts Breast Cancer Survival and Functionally Regulates Response to Chemotherapy. *Cancer Discov*. April 2011.

14. Cannarile MA, Weisser M, Jacob W, Jegg A-M, Ries CH, Rüttinger D. Colony-stimulating factor 1 receptor (CSF1R) inhibitors in cancer therapy. *J Immunother Cancer*. 2017;5:53.

15. Hodi FS, Ballinger M, Lyons B, et al. Immune-Modified Response Evaluation Criteria In Solid Tumors (imRECIST): Refining Guidelines to Assess the Clinical

Benefit of Cancer Immunotherapy. *J Clin Oncol Off J Am Soc Clin Oncol*. 2018;36:850-858.

16. Mulder WJM, Strijkers GJ, van Tilborg GAF, Griffioen AW, Nicolay K. Lipid-based nanoparticles for contrast-enhanced MRI and molecular imaging. *NMR Biomed*. 2006;19:142-164.

17. Cormode DP, Jarzyna PA, Mulder WJM, Fayad ZA. Modified natural nanoparticles as contrast agents for medical imaging. *Adv Drug Deliv Rev*. 2010;62:329-338.

18. Pérez-Medina C, Tang J, Abdel-Atti D, et al. PET Imaging of Tumor-Associated Macrophages with 89Zr-Labeled High-Density Lipoprotein Nanoparticles. *J Nucl Med Off Publ Soc Nucl Med*. 2015;56:1272-1277.

19. Pérez-Medina C, Binderup T, Lobatto ME, et al. In Vivo PET Imaging of HDL in Multiple Atherosclerosis Models. *JACC Cardiovasc Imaging*. 2016;9:950-961.

20. Weissleder R, Nahrendorf M, Pittet MJ. Imaging macrophages with nanoparticles. *Nat Mater*. 2014;13:125-138.

21. Guy CT, Cardiff RD, Muller WJ. Induction of mammary tumors by expression of polyomavirus middle T oncogene: a transgenic mouse model for metastatic disease. *Mol Cell Biol*. 1992;12:954-961.

22. Strachan DC, Ruffell B, Oei Y, et al. CSF1R inhibition delays cervical and mammary tumor growth in murine models by attenuating the turnover of tumor-associated macrophages and enhancing infiltration by CD8+ T cells. *Oncoimmunology*. 2013;2.

23. Stanley ER, Chitu V. CSF-1 Receptor Signaling in Myeloid Cells. *Cold Spring Harb Perspect Biol*. 2014;6:a021857.

24. Romano E, Schwartz GK, Chapman PB, Wolchock JD, Carvajal RD. Treatment implications of the emerging molecular classification system for melanoma. *Lancet Oncol*. 2011;12:913-922.

25. Hodi FS, Hwu W-J, Kefford R, et al. Evaluation of Immune-Related Response Criteria and RECIST v1.1 in Patients With Advanced Melanoma Treated With Pembrolizumab. *J Clin Oncol*. 2016;34:1510-1517.

26. Schwartz LH, Litière S, de Vries E, et al. RECIST 1.1 – Update and Clarification: From the RECIST Committee. *Eur J Cancer Oxf Engl 1990*. 2016;62:132-137.

27. Tazdait M, Mezquita L, Lahmar J, et al. Patterns of responses in metastatic NSCLC during PD-1 or PDL-1 inhibitor therapy: Comparison of RECIST 1.1, irRECIST and iRECIST criteria. *Eur J Cancer*. 2018;88:38-47.

28. Kanazawa H, Ohsawa K, Sasaki Y, Kohsaka S, Imai Y. Macrophage/Microglia-specific Protein Iba1 Enhances Membrane Ruffling and Rac Activation via Phospholipase C-γ-dependent Pathway. *J Biol Chem*. 2002;277:20026-20032.
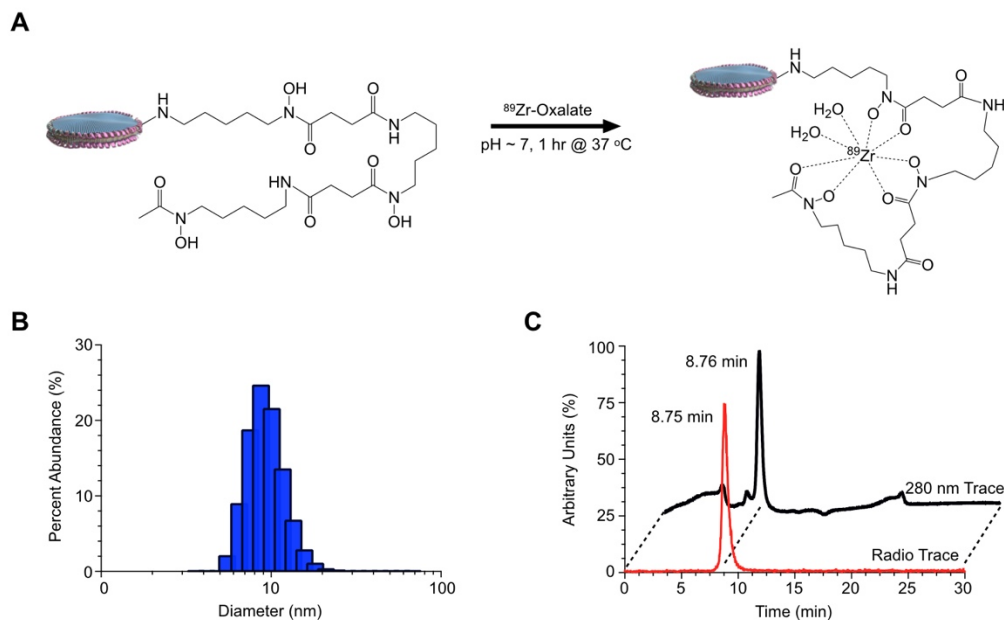
FIGURE LEGENDS

Figure 1. Synthesis and characterization of [89]Zr-HDL nanoparticles. (A) Radiolabeling synthesis conditions for the formation of [89]Zr-HDL nanoparticles. (B) Dynamic light scattering analysis of HDL nanoparticles exposed to labeling conditions. (C) RadioHPLC analysis illustrating chemical and radiochemical purity of [89]Zr-HDL nanoparticles.
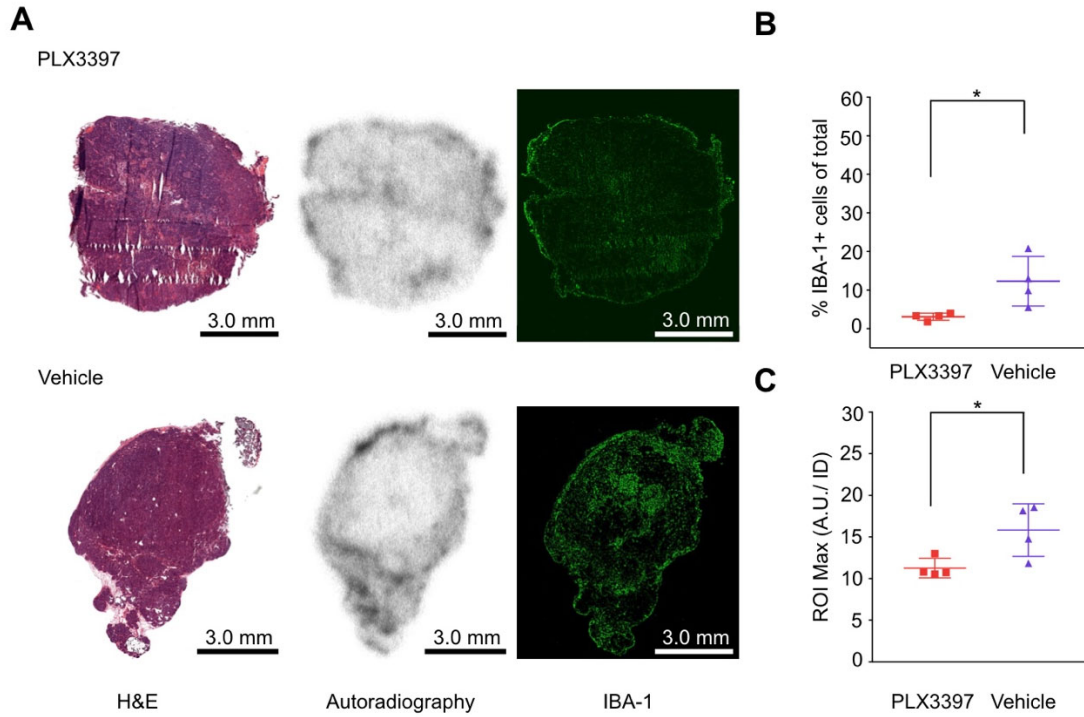
Figure 2. Ex vivo quantification of ^{89}Zr-HDL nanoparticle correlates with tumor associated macrophage density. (A) H&E, autoradiography, and immunofluorescence images of tumors excised from MMTV-PyMT mice. (B) Quantification of TAMs represented as percentage of total cells. (C) Maximum accumulation of ^{89}Zr-HDL nanoparticles within ROI on autoradiography, activity was normalized to the injected dose for each mouse. *P < 0.05.
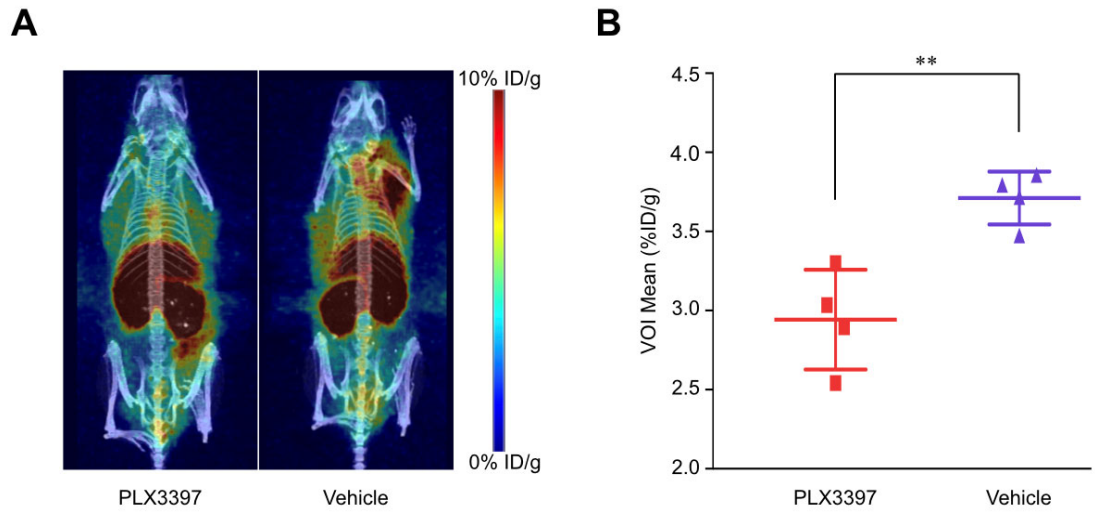
Figure 3. In vivo analysis of ^{89}Zr-HDL nanoparticles, visualized by PET/CT, showing reduced accumulation in mice treated with PLX3397. (A) PET/CT images representing ^{89}Zr-HDL nanoparticle distribution. (B) Quantification of ^{89}Zr-HDL nanoparticle uptake determined by drawing volume of interest over entire tumor burden. **P < 0.01

MATERIALS AND METHODS

Materials. 1-(4-Isothiocyanatophenyl)-3-[6,17-dihyroxy-7,10,18,21-tetraoxo-27-[N-acetylhydroxylamino) 6,11,17, 22 -tetraazaheptaeicosane]thiourea (DFO-p-NCS) was purchased from Macrocyclics, while phospholipid 1,2-dimyristoyl-*sn*-glycero-3-phosphocholine (DMPC) was purchased from Avanti Polar Lipids. Apolipoprotein A1 (APOA1) was collected from human plasma using a previously described protocol (*16*). Pexidartinib (PLX3397) was purchased from Selleck chemicals. All other reagents were purchased from Sigma Aldrich.

Isotope Production. The ^{89}Zr-oxalate was produced at Memorial Sloan Kettering Cancer Center (MSK) on an EBCO TR19/9 variable-beam energy cyclotron (EBCO Industries Inc.) via the ^{89}Y(p,n)^{89}Zr reaction and purified in accordance with previously reported methods to yield ^{89}Zr with a specific activity of 195−497 MBq/μg. Activity measurements were made using a Capintec CRC-15R Dose Calibrator (Capintec).

HPLC and Radio-HPLC. High-performance liquid chromatography (HPLC) was performed on a Shimadzu HPLC equipped with two LC-10AT pumps and an SPD-M10AVP photodiode array detector. Radio-HPLC was performed using a Lablogic Scan-RAM Radio-TLC/HPLC detector. Size exclusion chromatography (SEC) was performed using a Superdex 10/300 column (GE Healthcare Life Sciences) with PBS as the eluent at a flow rate of 1 mL min^{-1}.

Preparation of deferoxamine (DFO)-labeled HDL nanoparticles. HDL nanoparticles were prepared using a method previously reported (*17*). Briefly, 100 mg of DMPC was dissolved in chloroform and subsequently evaporated to form a thin lipid film. The film was rehydrated in 6 mL PBS at 35-40 ºC, before APOA1) was added to a final DMPC/APOA1 mass ratio of 2.5:1. The resulting solution was sonicated on ice for 15 minutes. Large aggregates were removed through centrifugation at 4,000 rpm for 5 min and the supernatant was filtered through a PES syringe filter (0.22 μm, 13 mm diameter, Celltreat Scientific Products). A buffer exchange was performed through spin filtration of the resulting suspension using a 10 kDa molecular weight cut-off (MWCO) Vivaspin 500 concentrator (GE Healthcare Life Sciences) at 5,000 rpm. The particles were dispersed in PBS and 0.1 M carbonate buffer (pH 9.0) was added until pH was adjusted to 8.7-9.0. DFO-p-NCS was then added in a 2:1 DFO to APOA1 mol ratio. The reaction was then incubated at 37 ºC for two hours, residual unbound DFO-p-NCS was removed through spin filtration (10 kDa MWCO) and the particles were subsequently suspended in PBS and passed through a 0.22 μm PES syringe filter. Size distribution analysis of the resulting nanoparticle suspension was measured using dynamic light scattering (DLS) on a Malvern Zetasizer (Malvern Instrument Ltd.) in triplicate, at 25 ºC allowing equilibration for 120 seconds, with a 173º angle of detection.

Radiolabeling of DFO-HDL nanoparticles. The ^{89}Zr-oxalate solution was neutralized to a pH of 7 using 1.0 M Na_2CO_3. Subsequently, 250 μL of HDL nanoparticles with an approximate concentration of 2.0 mg/mL with respect to APOA1 was added to the neutralized ^{89}Zr. The reaction solution was incubated at 37 °C for 1 hour, free ^{89}Zr was

then removed via centrifugation using a 10kDa MWCO vivaspin filtration tube. The ^{89}Zr-HDL nanoparticles were diluted in sterile PBS and filtered through a PES syringe filter (0.22 μm). A radiochemical purity of > 99% for the ^{89}Zr labeled HDL nanoparticles was determined by RadioHPLC.

Animal model. 6-8 week old female transgenic FVB/N-Tg (MMTV-PyMT)634Mul/J mice were purchased from Jackson Laboratories. Animals develop mammary fat pad tumors which metastasize to the lung. At 11-12 weeks of age, once tumors had reached approximately 5.0 mm in diameter, the mice were randomized by tumor burden and administered either PLX3397 (50 mg/kg), formulated in 0.5% (hydroxypropyl)methyl cellulose (HPMC) and 1.0% polysorbate 80, or vehicle via daily oral gavage for 5 days. Animal experiments were done in accordance with protocols approved by the Institutional Animal Care and Use Committee of Memorial Sloan Kettering Cancer Center and followed National Institutes of Health guidelines for animal care.

PET/CT imaging of ^{89}Zr-HDL nanoparticles. On the fifth day of PLX3397 or vehicle administration, mice were injected with approximately 5.55MBq of ^{89}Zr-HDL nanoparticles in 200 μL PBS solution via the lateral tail vein. Animals were anesthetized with isoflurane (Baxter Healthcare)/oxygen gas mixture (2% for induction, 1 % for maintenance), and subsequently imaged using an Inveon PET/CT scanner (Siemens Healthcare Global) at 24 hours post injection. Whole body PET static scans recording a minimum of 30 million coincident events were performed. The energy and coincidence timing windows were 350−650 keV and 3.432 ns, respectively.

Image analysis and quantification. Images were analyzed using ASIPro VMTM software (Concorde Microsystems) or 3D Slicer, version 4.10 (www.slicer.org). Quantification of tumor-associated activity was performed through a combination of manual and semi-automatic segmentation techniques in 3D Slicer used to define tumor volumes within the cervical, thoracic, and inguinal mammary glands. Mean uptake within each tumor segment was quantified in percentage of the injected dose per gram of tissue (%ID/g) (*18*). No partial volume corrections were applied.

Autoradiography. To determine intratumoral radiotracer distribution, digital autoradiography was performed by placing tissue sections in a film cassette against a phosphorimaging plate (Fujifilm BAS-MS2325; Fuji Photo Film) for approximately 24 hours at -20 °C. Phosphorimaging plates were read at a pixel resolution of 25 µm with a Typhoon 7000IP plate reader (GE Healthcare Life Sciences). Quantification was carried out using ImageJ software (*19*).

Tissue staining and microscopy. Once counted and weighed the excised tumors were embedded in optimal cutting temperature (OCT) medium, frozen in dry ice, and stored at -20 °C. The tumors were then sectioned at 10 µm thickness. Staining was carried out using the automated Discovery XT processor (Ventana Medical Systems) at the Molecular Cytology Core Facility at MSK. Stained sections were digitalized using a MIRAX Slide Scanner (3DHISTECH). Thresholding was performed on IBA-1 (green, Atto-488) and DAPI (blue) areas, the percentage of IBA-1 positive cells

compared with total cells was determined for each section using an automated script, written by the Molecular Cytology Core Facility at MSKCC, in ImageJ. The PLX3397 treatment and control groups are each represented by 4 mice, at least 5 sections for each mouse was used for quantification (total of 20 sections for each cohort).

Statistical analysis. Data was expressed as mean ± standard deviation, statistical analysis was performed on each data set using GraphPad Prism, Version 7.0e using parametric unpaired t-tests, assuming unequal standard deviations between the two cohorts. Results were considered statistically significant with P values < 0.05.
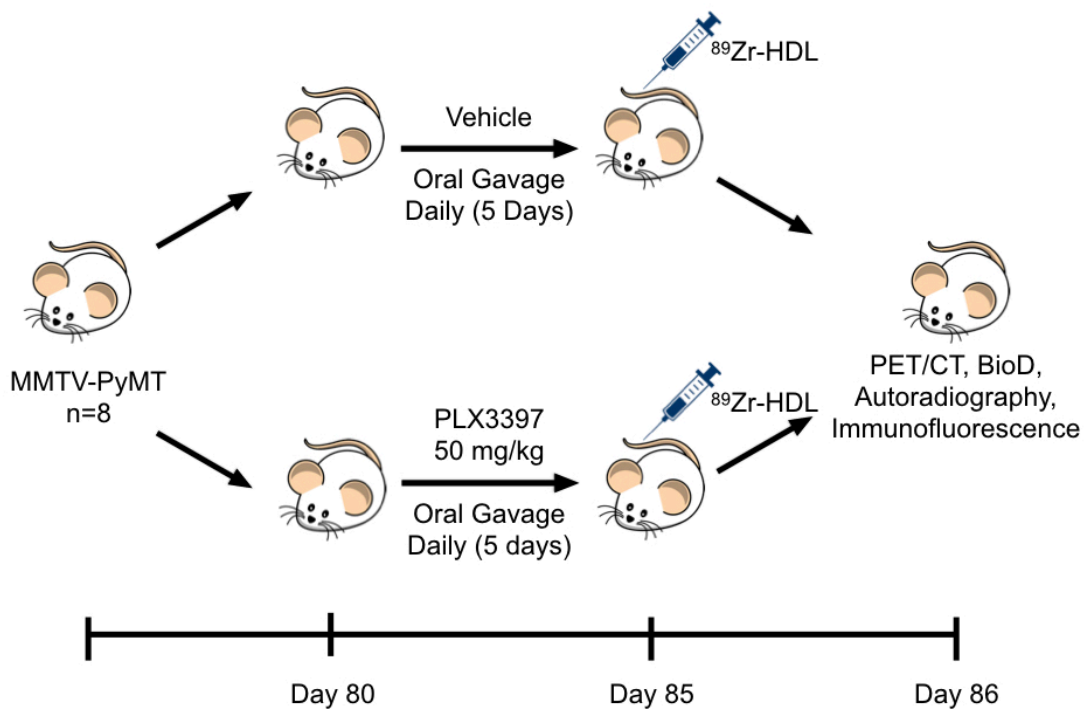
Supplemental Figure 1. Methodology for the *in vivo* assessment of ^{89}Zr-HDL nanoparticles as reporter for monitoring response to the CSF1R inhibitor, pexidartinib.
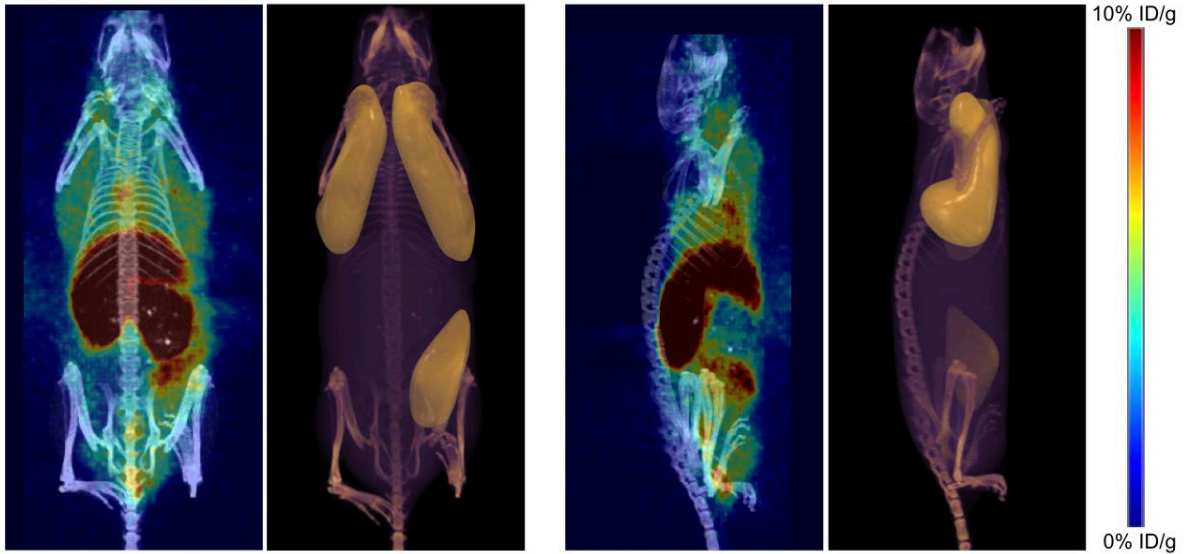
Supplemental Figure 2. PET/CT images of ^{89}Zr-HDL nanoparticles and the corresponding VOI drawn to quantify nanoparticle accumulation Quantification of ^{89}Zr-HDL nanoparticles in PET/CT images.
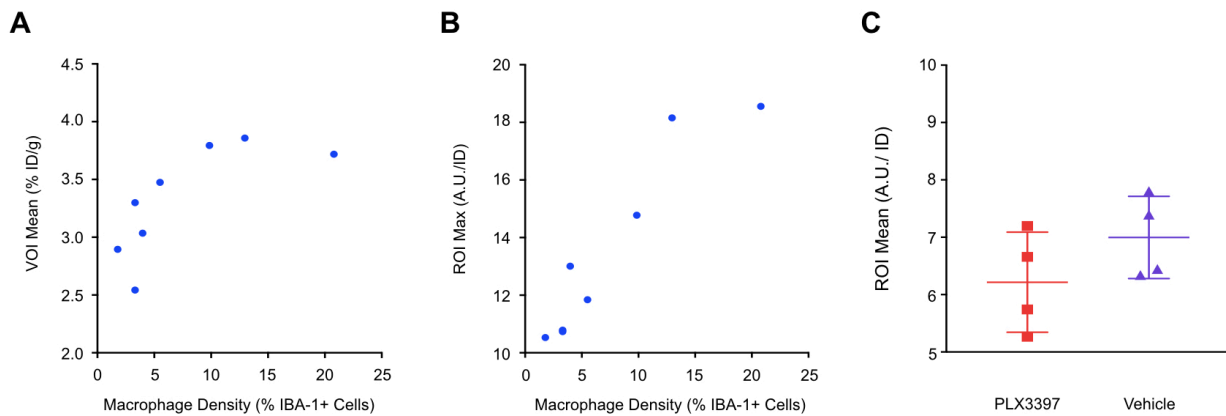
Supplemental Figure 3. Ex vivo analysis of tumor sections. A) Correlation between VOI mean from PET/CT images and macrophage density from immunofluorescence. B) Correlation between ROI max from autoradiography and macrophage density from immunofluorescence. C) Autoradiography quantification, average accumulation within ROI for tumor sections.